Scaling of Lennard-Jones liquid elastic moduli, viscoelasticity and other properies along fluid-solid coexistence

D.M. Heyes* and D. Dini†

Department of Mechanical Engineering, Imperial College London, Exhibition Road, London, SW7 2AZ,United Kingdom

A.C. Brańka‡

Institute of Molecular Physics,Polish Academy of Sciences, M. Smoluchowskiego 17,60-179 Poznań, Poland§

(Dated: January 3, 2015)

Abstract

Static and dynamical properties of the Lennard-Jones (LJ) fluid along the fluid-solid coexistence line are determined by Molecular Dynamics simulation. A number of properties, such as the radial distribution function, Einstein frequency, mean force, root mean square force, and normalized time correlation functions are shown to be essentially invariant or structurally isomorphic along this line when scaled by so-called macroscopic variables (MRU). Other quantities subject to MRU such as the potential energy, pressure and infinite frequency compressional modulus are not constant along this line of states but can be reproduced using simple formulae of the form for Roskilde fluids. The elastic moduli fall within the domain of isomorphism theory. A generalized Cauchy relationship in which the infinite frequency longitudinal modulus is proportional to the longitudinal modulus of the fluid was found to be obeyed very well for the LJ fluid phase along this coexistence line.

PACS numbers:

*Electronic address: david.heyes@rhul.ac.uk

†Electronic address: d.dini@imperial.ac.uk

‡Electronic address: branka@ifmpan.poznan.pl

§Submitted to the 'AUXETICS 2014' special issue in Physica Status Solidi B

I. INTRODUCTION

Auxetic and other negative-valued material properties of solids are active areas of research [1]. Their existence in fluid phases is an intriguing possibility which has received little attention. The fluid state of matter has quite distinct mechanical behaviour to that of the solid (crystalline) form. Fluids are not capable of sustaining indefinitely a stress after the application of a step in strain, so any such response would be a transient. However, on a short time scale it is well-known from the pioneering work of J. C. Maxwell, [3] that fluids behave with a solid-like or 'viscoelastic' response. He proposed that the shear viscosity, η_s, of a fluid can be written as, $\eta_s = G_\infty \tau$, the product of an elastic modulus, G_∞ and a relaxation time, τ. The liquid behaves as a solid on time scales much shorter than τ. This is of practical significance as the mechanical properties of important every-day states of matter such as glasses, gels or granular beds can for practical purposes be treated as solids, even though the microstructure is liquid-like and they are strictly speaking metastable assemblies of particles. Any stressed state will eventually relax over time to an unstressed state. For simple liquids, τ is of order a picosecond, while for these other materials it can be days, years or even centuries. It has proved particularly problematic to develop statistical mechanical theories and descriptions for the dense superctitical fluid and liquid states, compared to dilute gases and the solid state.

Some important theoretical developments in the statistical mechanics of the dense fluid state have used a reference model fluid as a starting point. Within this class, the soft sphere potential has proved an important model interaction for simple and complex fluids (*e.g.*, hydrogels, [2]). The soft sphere or inverse power, IP, pair potential is of the form $\sim r^{-n}$, where r is the distance between the two centres of mass, and the value of the exponent, n, governs the potential stiffness ($n \to \infty$ is the hard sphere potential). In the last decade there have been

many publications applying soft sphere scaling in one form or another to a range of physical properties. The scale invariance of the IP potential lends itself to such an application. Hidden **scale** invariance in van der Waals fluids (*i.e.*, those not significantly hydrogen bonded) is found in material properties if plotted appropriately. A motivation for this is it provides an improved understanding of observed trends in experimental systems, and from a practical point of view, can reduce the number of state points that need to be considered. Roland *et al.*,[4, 5] found that viscosity data for a series of real oils collapsed onto common curves using the IP scaling parameter, $(T/T_R)(\rho_r/\rho)^\gamma$ where T_R and ρ_R are the temperature and density of a reference system, respectively. The exponent, γ is exactly $n/3$ for an IP fluid but has to be treated as a fit parameter for real experimental data as the effective value of n for each molecule is not known in advance, and these systems will not be represented exactly by the inverse power potential. This density-temperature scaling procedure [6] was subsequently applied to collapse onto a single master curve the self-diffusion coefficients of model Lennard-Jones liquids [7], and relaxation and thermodynamic data of experimental systems [8]. Dyre and co-workers, (see for example, Refs. [9–14]) provided additional statistical mechanical foundations to the extension of scaling concepts to real van der Waals fluids. They invented the classification of 'strongly correlating' or Roskilde fluids, which are liquids where the equilibrium virial-potential energy correlation coefficient is about or at least 0.9 (this number is always 1 for inverse power liquids for all fluid state points) which give rise to lines of density-temperature states which inherit a number of soft sphere scaling properties, and were called *isomorphic* states. This approach has allowed lines of nearly invariant values for structural, static and dynamical properties in reduced units to be established, which has *inter alia* helped to explain the origins of empirical correlations between these quantities discovered in the past [15, 16].

The Lennard-Jones potential has a form which has made it suitable to represent well the

effective pair interaction between molecules in typical dense 'van der Waals' fluids such as argon and small molecules. The remit of this work is to explore further aspects of the Roskilde fluid categorisation for the Lennard-Jones system along the fluid-solid coexistence boundary. Notably the infinite frequency elastic moduli which are relevant to mechanical properties, and time correlation functions whose integral leads to the transport coefficients are considered. The term, 'fluid' is used here rather than 'liquid' as many of the data points considered are at a temperature above the critical temperature. The focus is on to what extent can the physical properties of this set of temperature-density states be collapsed onto a single master curve. In Sect. II the theoretical background to this work is covered, which includes an analysis of literature simulation data on the LJ fluid-solid coexistence boundary, and an explanation of the appropriate set of reduced units relevant to the isomorphism condition. In Sect. III the results of Molecular Dynamics simulations of the fluid along the fluid-solid coexistence boundary are presented and analysed for signs of isomorphism. Conclusions are made in Sect. IV.

II. THEORETICAL BACKGROUND

First aspects of the Lennard-Jones phase coexistence behavior are discussed, and then the subject of property scaling is covered.

A. The Lennard-Jones phase behavior

The focus here is on the Lennard-Jones (LJ) fluid in which the molecules interact with the pair potential, $\phi(r) = 4\epsilon[(\sigma/r)^{12} - (\sigma/r)^6]$, where ϵ and σ define the energy and length scales of the molecule, respectively. The first term represents the *repulsive* and the second term the *attractive* part of the intermolecular interaction. For the pure LJ system typical values of the critical point parameters for temperature, reduced density and pressure are, T_c, ρ_c and P_c are 1.3120(7), [17, 18], 0.316(1), [19] and 0.141(1), [20] respectively. The triple point temperature and density are *ca.* 0.69 and 0.85, respectively. [21] Lennard-Jones reduced units (see below) are used.

Figure 1 shows the vapour-liquid coexistence boundary (black symbols) and the liquid-solid phase boundary (blue symbols) for number density, ρ against pressure, P using molecular simulation numerical data taken from literature sources. As will be seen that owing to the absence of data points near the critical point it cannot be reached directly by simulation or in fact experiment. Figure 2 concentrates on the fluid-solid phase boundary as a function of density and temperature. **It has been proposed recently that the coexistence density of the liquid and solid phases for the LJ conform to the formula, [22–25]**

$$T = A\rho^4 - B\rho^2, \tag{1}$$

where A and B are constants which can be fitted separately to the fluid and solid numerical data. Making T the independent variable, from Eq. (1), then

$$\rho = (\frac{B + \sqrt{B^2 + 4AT}}{2A})^{1/2}. \tag{2}$$

Equations (1) and (2) are referred to as the $M42$ model, **where the '4' and '2' are the exponents of the density**. The analytic form of Eq. (1) anticipates one of wider applicability for other static properties, in which the ρ^4 and ρ^2 terms derive from the repulsive and attractive parts of the potential, respectively. This will be discussed further below. Another analytic form we propose here is,

$$T = C + D\rho^4, \tag{3}$$

where C and D are constants which can be fitted to numerical data, and where

$$\rho = ((T - C)/D)^{1/4} \tag{4}$$

Equations (3) and (4) are referred to as the $M40$ model, **where the '4' and '0' are the exponents of the density**. Equations Eq. (3) and (4) are based solely on the repulsive part of the LJ potential (*i.e.*, $n = 12$ and hence $n/3 = 4$) and treat the effect of the attractive part of the potential as a mean field 'offset' in the location of the phase boundary. Figure 2 shows temperature as a function of density, $T(\rho)$. The $M42$ and $M40$ analytical formulae follow the numerical data very well for all temperatures considered for the solid coexistence line, but below a temperature of $\simeq 0.95$ (towards the triple point) both formulae underestimate the coexistence temperature for the liquid. The corresponding solid line fits the simulation data very well even in this temperature range, **with** $M40$ **being slightly better than** $M42$ **at the lowest temperatures**. At high temperature T and ρ the repulsive part of the LJ potential dominates, as evident in the analytic form of Eq. (1).

The soft-sphere system is a useful reference system for the LJ in this context, and its fluid-solid coexistence densities have been determined using the Gibbs-Duhem equation coupled with Molecular Dynamics simulation.[26]

Figure 3 shows ρ as a function of T. The formulae in Eqs. (2) and (4) are plotted together with the numerical data on this figure. These formulae are useful as input for tracing out the coexistence line using molecular simulation for temperatures in excess of *ca.* $T < 0.95$. The soft sphere derived coexistence densities in LJ units for $n = 12$ are approximately represented by the curves, $0.8238T^{1/4} + 0.069$ and $0.8549T^{1/4} + 0.069$ (note the shift factor) based on the soft sphere coexistence densities at $T = 1$ taken from Refs. [27, 31], which are also given on Fig. 3. The shift factor is to ensure reasonable agreement at high temperature between the soft sphere and Lennard-Jones curves. It is clear that at no temperature can the effect of the attractive part of the LJ potential be ignored as far as the coexisting densities are concerned. **Note that the low temperature region is expanded in Fig. 2 by the lin-log scales.**

The dependence of pressure (P) on density and temperature along the LJ fluid-solid coexistence line has been investigated in the literature, and a number of semi-empirical formulae for $P(T)$ been proposed. For example, as a fit to simulation data, Agrawal and Kofke, [27] represented the coexistence pressure by

$$P = \beta^{-5/4} \exp(-0.4759\beta^{1/2})(16.89 + E\beta + F\beta^2) \tag{5}$$

where $\beta = 1/k_B T$, $E = -59$ and $F = 12$. Mastny and de Pablo, [28] give values for $E = -8.2269$ and $F = -2.3980$ based on their numerical data. The first factor in the above equation, $16.89\beta^{-5/4}$, is that of the soft-sphere systems with exponent, $n = 12$, dependence [29]. There are other $P(T)$ fluid-solid coexistence formulae in the literature. [30] The soft sphere

coexistence pressure is 23.7 at $T = 1$, [31] where the soft sphere potential can be written as, $\epsilon(\sigma_S/r)^{12}$ for $n = 12$. Converting to the corresponding Lennard-Jones potential form, $4\epsilon(\sigma_{LJ}/r)^{12}$ we have, $\sigma_{LJ} = \sigma_S/4^{1/12}$ so, $P = 16.76\ T^{5/4}$ in LJ units for soft sphere scaling. The empirical Simon equation for real solids also takes the form $P \propto T^{\alpha}$ along the melting line (see for example Ref. [32]). Figure 4 shows that this 'soft sphere' equation of state overestimates the pressure for temperatures below *ca.* 100 but the two curves converge for higher temperatures. The offset caused by the attractive part of the LJ potential has a non-negligible effect on the value of the coexistence pressure up to very high temperatures for real substances (*e.g.*, $\sim 11,000$ K for argon, taking $\epsilon/k_B = 120$ K). Unlike the coexisting densities of Fig. 3, at high temperature the effect of the attractive part of the LJ potential on the pressure can in practice be ignored. The $P(T)$ curve requires no shift factor to obtain convergence of the soft sphere and Lennard Jones curves at high temperature. Coexisting densities depend on the Gibbs free energy (and pressure) of the two phases being equal while the pressure is the derivative of the free energy with respect to volume, so any constant term present in the analytic form of the free energy to account for the attractive part of the potential will disappear on taking any derivative of the free energy. Figure 4 also shows data for the repulsive LJ or WCA fluid at coexistence with the solid [33]. The data for this system extend to low temperatures, and agree quite well with the soft sphere line (in red). This is perhaps not surprising as the WCA and $n = 12$ soft sphere potential are more similar than either is to the LJ potential form.

B. Types of Reduced Units

So far only Lennard-Jones reduced units have been considered. In the past an alternative reduction has been proposed a number of times for various properties, based on macroscopic and fundamental ('real') units (see for example, Refs. [40–44]). This is based in potential-independent quantities rather than on molecular or the effective pair potential parameters. This treatment has recently been given theoretical justification by the Roskilde group of Dyre and coworkers who have shown that such quantities can be almost constant ('invariant'), or readily computed failing that, along certain density-temperature ('isomorphic') lines on the phase diagram of the LJ fluid and other model molecule fluid. Using their notation, the reduced quantities ($\tilde{X}$) for some relevant quantities are defined as follows,

$$\begin{aligned} r &= \rho^{-1/3}\tilde{r}, \\ u &= k_B T \tilde{u}, \\ P &= \rho k_B T \tilde{P}, \\ t &= \rho^{-1/3} m^{1/2} (k_B T)^{-1/2} \tilde{t}, \\ D &= \rho^{-1/3} m^{-1/2} (k_B T)^{1/2} \tilde{D}, \\ \eta &= \rho^{2/3} m^{1/2} (k_B T)^{1/2} \tilde{\eta}, \\ \lambda &= \rho^{2/3} m^{-1/2} (k_B T)^{1/2} \tilde{\lambda} k_B \end{aligned} \tag{6}$$

where X is the quantity in real units, u is the potential energy per particle, $\rho = N/V$ is the number density in real units, m is the mass of the molecule, and there are N molecules in volume V. The self-diffusion coefficient is denoted by, D, and the viscosity is η (η_s for the shear viscosity and η_b for the bulk or compressional viscosity). The thermal conductivity is denoted by λ. Each quantity, X, on the left hand side of Eq. (6) is in real (*e.g.*, S.I.) units while its reduced version $\tilde{X}$ given on the right hand side is dimensionless, the units being taken up by the remaining quantities in each formula. **As the '$\tilde{X}$' scaled quantities are**

a mixture of macroscopic intensive thermodynamic quantities (*i.e.*, ρ and T) and microscopic quantities such as m and k_B it is approporiate to refer to them as 'M' reduced units or MRU for short.

For model fluids such as the Lennard-Jones example it is is customary to express its physical properties in molecular pair potential parameter units (sometimes identified with an '$*$' superscript), as we have used in the previous subsection. The same quantities expressed in pair potential units are,

$$\begin{aligned} r &= \sigma r^*, \\ \rho &= \sigma^{-3}\rho^*, \\ T &= \epsilon T^*/k_B, \\ u &= \epsilon u^*, \\ P &= \epsilon\sigma^{-3}P^*, \\ t &= \sigma(m/\epsilon)^{1/2}t^*, \\ D &= \sigma\epsilon^{1/2}m^{-1/2}D^*, \\ \eta &= \sigma^{-2}\epsilon^{1/2}m^{1/2}\eta^*, \\ \lambda &= \sigma^{-2}m^{-1/2}(T)^{1/2}\lambda^* k_B. \end{aligned} \tag{7}$$

Again the quantities, X, on the left of the above equation are in real units while X^* are unitless, the units coming from the remaining terms based on the molecule's description.

Equating the same quantities in Eqs. (6) and (7) and rearranging gives,

$$\begin{aligned} \tilde{r} &= \rho^{*1/3}r^*, \\ \tilde{u} &= u^*/T^*, \\ \tilde{P} &= P^*/\rho^*T^* = Z, \end{aligned}$$

$$
\begin{aligned}
\tilde{t} &= \rho^{*1/3} T^{*1/2} t^*, \\
\tilde{D} &= \rho^{*1/3} T^{*-1/2} D^*, \\
\tilde{\eta} &= \rho^{*-2/3} T^{*-1/2} \eta^*, \\
\tilde{\lambda} &= \rho^{*-2/3} T^{*-1/2} \lambda^*
\end{aligned} \tag{8}
$$

and for completeness, $\beta = 1/k_B T$, so $\beta^* = 1/T^*$. Both LJ reduced and MRU scaling will be used to test for isomorphism in Sect. III. As the Lennard-Jones fluid is being considered here, the asterisk is dropped henceforth for reasons of compactness of notation.

Statistical mechanics suggests why the MRU representation has proved so effective in collapsing experimental and simulation data onto master curves. Consider the potential energy per particle, for example, which is defined from the following NVT ensemble average,

$$
\tilde{u} = u\beta = \frac{\rho^{n/3}}{T} \frac{\int \underline{\tilde{r}}^N \tilde{u}(\underline{\tilde{r}}^N) exp(-\frac{\rho^{n/3}}{T} \sum_{ij} (\frac{1}{\tilde{r}_{ij}})^n + \frac{\rho^{m/3}}{T} \sum_{ij} (\frac{1}{\tilde{r}_{ij}})^m)}{\int \underline{\tilde{r}}^N exp(-\frac{\rho^{n/3}}{T} \sum_{ij} (\frac{1}{\tilde{r}_{ij}})^n + \frac{\rho^{m/3}}{T} \sum_{ij} (\frac{1}{\tilde{r}_{ij}})^m)} \tag{9}
$$

where $\underline{\tilde{r}}^N \equiv \underline{\tilde{r}}_1, \underline{\tilde{r}}_2 \cdots \underline{\tilde{r}}_N$, is a general point in the configurational phase space of the N-molecules, $\underline{r}_{ij} = \underline{r}_i - \underline{r}_j$ and $r_{ij} = |\underline{r}_{ij}|$ is the distance between molecules i and j. The more general $n : m$ notation is used (the $12 : 6$ special case is the Lennard-Jones potential). For the special case of the soft sphere potential ($\epsilon(\sigma/r)^n$) (by omitting the m-terms in Eq. (9)), the MRU potential energy, $\tilde{u}$, has the same value along the $\rho^{n/3}/T = constant$ line. These states are said to be *isomorphic* or as we suggest, *structurally isomorphic* to be more specific, because when the coordinates are MRU nondimensionalized by the density, the probability distribution of the configurations in reduced units, $P(\underline{\tilde{r}}^N)$, is the same for all states along the isomorphic line. To say that a *quantity* is 'isomorphic' means that it has a constant value in MRU along a set of structurally isomorphic states, but this does not automatically follow from structural isomorphism, as will be shown below.

The more general $m:n$ case two term pair potential it is not so simple to treat. Even though $\rho^{n/3}/T$ may be equal for two density-temperature states on the phase diagram, the quantity, $\rho^{m/3}/T$ (where $m \neq n$) will not be the same. The contribution from the repulsive and attractive parts of the potential to a given quantity (*e.g.*, u) will be weighted differently in the two cases. The two states may be structurally isomorphic to a good approximation, but the values of $\tilde{u}$ for the total potential energy will not be the same. In the perturbation theory of liquids it is assumed that the structure of the liquid is determined by an effective short range repulsive potential, which in the case of the Weeks-Chandler-Andersen theory of the Lennard-Jones fluid, is a combination of the r^{-12} and r^{-6} terms, rather than solely the r^{-12} part of the potential which underpins the present analysis. In the present context, this would be tantamount to replacing the term $\sum_{ij}(\frac{1}{\tilde{r}_{ij}})^m$ in Eq. (9) by a (perhaps solely density dependent) constant, which will cancel out between the numerator and denominator. This, one might consider rather drastic, approximation would lead to approximate isomorphism even in the $n:m$ pair potential case. Its practical benefits can only be confirmed by applying the MRU reduction of experimental or molecular simulation data. This was the approach adopted by Coslovich and Roland, [46] who represented an $n:m$ potential fluid by a repulsive inverse power fluid with the attraction term approximated by a uniform background term, $\phi(r) \sim r^{-k} + constant$, where k is another soft sphere exponent (it could transpire that $k \simeq n$ in favorable cases). The physical properties of the soft-sphere fluid are now known essentially analytically for most of the exponent range (except very close to $n = 3$). [47] The prediction for Roskilde fluids and solids is that Lennard-Jones isomorphs follow the state point path defined through, [24]

$$\frac{A\rho^4 - B\rho^2}{T} = constant \tag{10}$$

where the constants, A and B need to be computed by simulation.

C. Dynamical and transport properties

The transport coefficients, D, η_s, η_b and λ were calculated by MD using the standard route of integrating the appropriate time correlation function in the Green-Kubo formulae. [48] The transport coefficient is generically represented by $M\tau$, where M is **an infinite frequency** 'modulus' and the relaxation time, τ, is the integral under a time correlation function (TCF) normalized to unity at time, $t = 0$. For a given property, X, the relaxation time is the integral of a normalised time correlation function, $C_X(t)$ which is the linear response relaxation function in the case of a transport property. Then, $\tau = \int_o^\infty C_X(t)dt$, where $C_X(t) =< X(t)X(0) > / < X(0)^2 >$. The **infinite frequency** elastic and thermal moduli were calculated from the $t = 0$ value of the unnormalized TCF, [49] and from the formulas specific to the LJ fluid given in Ref. [51]. For the shear viscosity, $M \equiv G_\infty$, the infinite frequency shear elastic modulus. For the bulk or compressional viscosity, $M \equiv K_\infty - K_0$, the difference between the infinite and zero frequency **isothermal** bulk moduli.

In the next section a wide range of physical of LJ fluid physical properties along the fluid-solid phase boundary are presented which were determined by Molecular Dynamics (MD) simulations carried out for this work.

III. RESULTS AND DISCUSSION

Molecular Dynamics (MD) simulations were carried out using the isotropic Lennard-Jones potential. The quantities presented are given in the usual LJ reduced units (*i.e.*, $\sigma = 1$, $\epsilon = 1$ and the mass of the molecule, $m = 1$), as discussed in the previous section. The truncation distance for the pair interaction contribution to the potential energy and virial was $r_c = 3.5$ with the usual long range correction formulas added in a mean field way, [52] to take account of those interactions not specifically computed. The critical temperature of the LJ system is known to be sensitive to truncation and various tapered modifications, [53] and the system simulated here is a compromise to represent the infinite range LJ potential as best as possible at reasonable computational cost. The reduced time step was $0.004/\sqrt{T}$ and simulations were conducted for up to 10^6 time steps during the post-equilibration stage at each state point. The number of particles in the simulation cell was 4000 or $10,976$, to minimise finite size effects along this high density line, especially at low temperature. The state points simulated were a selection of those given in Table. II of Ref. [21, 39]. State points with (T, ρ) values ranging from $(0.692, 0.847)$ to $(40.0, 2.01)$ were considered.

Figure 5 shows the radial distribution function, $g(r)$ for three widely separated fluid state points along fluid-solid coexistence. The top set of curves is where distance, r, is in LJ units, which shows quite distinct curves. When plotted as a function of $\tilde{r}$, these curves superimpose very well, strongly suggesting that the fluid states along the fluid-solid coexistence line are to an excellent degree structurally isomorphic. Bøhling *et al.* explored the significance of superimposable radial distribution functions in the context of isomorphism [54]. Figure 6 shows the corresponding $g(r)$ plots for solid state points. The three state points show the signature

of a crystalline structure with multiple peaks some distance from the molecular diameter (*i.e.*, $r = 1$). Along the nominal fluid line the free energy difference between the fluid and coexisting solid is sufficiently small that the system can overcome a practical activation energy to form a crystalline state which is possibly metastable, although there is some uncertainty in the true values of the coexisting fluid and solid densities for the LJ system. Again excellent structural isomorphism is evident in the practical superposition of the three solid state $g(r)$ functions at least as far as $r = 5$. **Isomorphs of crystals were studied recently by MD simulation in Ref. [55], where a very good collapse of structure and dynamics, in fact better than in the liquid phase, was found**.

Figure 7 shows various static averages, expressed in macroscopically reduced form for the LJ system along the fluid side of fluid-solid coexistence. These include, the mean force on the molecule, $< \tilde{F} >$, the root mean square force on the molecule, $< \tilde{F}^2 >^{1/2}$ and the Einstein frequency, $< \tilde{\omega}_E >$,[56] where

$$\omega_E^2 = \frac{4\pi\rho}{3m} \int_0^\infty dr\ r^2 \left(\phi''(r) + \frac{2\phi'}{r} \right) g(r). \tag{11}$$

These quantities are probably dominated by the repulsive part of the potential, so from the discussion in the previous section it is expected that the derived properties most sensitive to the repulsive term in the potential will show the greatest invariance with density when expressed in MRU reduced form. The figure shows that the force and root mean square force, and Einstein frequency manifest a weak density dependence when expressed in MRU form, a result which is consistent with the dominance of the repulsive part of the part potential in governing these properties.

The time dependent functions are considered now. The normalised velocity autocorrelation

function,[57] $C_v(t) =< \underline{v}(0) \cdot \underline{v}(t) > / < \underline{v}^2(0) >$, is plotted for three well separated state points exhibiting a solid or crystalline structure in Fig. 8. This shows the negative or rebound region which is indicative of a caged molecule. The $C_v(t)$ obeys $\tilde{t}$ or 'isochronal' scaling, [16, 62] very well, as may be seen in the coincident three lower curves of Fig. 8. The top set of curves are the C_v plotted against time in LJ reduced units, and the bottom curves are the same quantities plotted using the macroscopically reduced time, $\tilde{t}$. Figure 9 shows the corresponding force autocorrelation functions, $C_F(t) =< \underline{F}(0) \cdot \underline{F}(t) > / < \underline{F}^2(0) >$, which also collapse with MRU at essentially all times. The corresponding **total** shear stress autocorrelation functions, [58] $C_s(t) =< P_{xy}(0)P_{xy}(t) > / < P_{xy}^2(0) >$ where P_{xy} is the xy component of the pressure tensor **(including the kinetic and interaction parts)**, are given in Fig. 10 for the three solid state points. These monotonically decaying functions expressed in terms of $\tilde{t}$ are hardly distinguishable on the lower frame of the figure. The deviatoric pressure ($X \equiv P(t) - < P >$) autocorrelation function, [61] for fluid states are given in Fig. 11. The heat flux autocorrelation functions, $C_{La}(t)$ for the three solid state points are given in Fig. 12.

Therefore to conclude this section, it is noteworthy that the normalised time correlation functions relevant to transport coefficients along the fluid-solid coexistence line are invariant when expressed in terms of MRU time. Hence the relaxation times, $\tilde{\tau}$ are invariant or isomorphic, as each is the integral of the normalised time correlation (relaxation) function. Therefore the state dependence of a transport coefficient will follow that of the modulus, M (a static property) using the exact Maxwell formula. It might be argued that the the MRU scaling of the radial distribution functions in the solid state in Fig. 6 is just the affine scaling one would expect for a crystalline sample. However, its application in the fluid state (see Fig. 5) cannot be so readily explained away. Also the excellent MRU scaling of time dependent properties as demonstrated in Figs. 8-12 cannot be so easily discounted.

For static quantities, X, which have significant contributions from the attractive part of the potential ($e.g.$, potential energy per particle, configurational part of pressure, and the elastic and thermal moduli) they should take the following analytic form which is a consequence of structural isomorphism exhibited by these systems,

$$\tilde{X} = A\rho^4 + B\rho^2, \tag{12}$$

where A and B are temperature independent constants. **The relationship in Eq. (12) we think may follow from the dominance of the r^{-12} term in the LJ potential in determining the structure and hence $g(r)$, which is consistent with classical perturbation theory, although we note the simulation and conclusions of Ref. [25] lead one to conclude that the explanation may not be so simple ($i.e.$, in by treating the repulsive and attractive parts of the LJ potential separately in this context).** It is worth noting that Rosenfeld proposed the same analytic form, where X is the pressure, in 1974 [59, 60] for the melting line properties, using a hard sphere reference fluid. Even though the states may be essentially structurally isomorphic these derived quantities will not give density independent $\tilde{X}$ because of the different density dependencies of the repulsive and attractive components, encapsulated in Eq. (12). Nevertheless, the simple analytic form in Eq. (12) is a significant step forward in our predictive capacity, as once A and B are determined (in principle) from two state points, the value of $< X >$ is predicted along an isomorphic line of state points. As a specific example, Fig. 13 shows the potential energy per particle, and its repulsive and attractive components as a function of density along the fluid-solid coexistence line obtained by the MD simulations carried out in this work. A previously introduced formula, [62, 63],

$$u = A_r\rho^4 - B_a\rho^2, \tag{13}$$

where A_r and B_a are constants was fitted to the simulation data is also shown on the figure.

Another formula,

$$u = C_r\rho^4 - D_a, \tag{14}$$

where C_r and D_a are constants, is also plotted on the figure. The formula in Eq. (13) fits the MD data very well, and better than Eq. (14). Also the individual terms for the repulsive and attractive parts of u given in Eq. (13) predict well with the repulsive and attractive components of the simulation data potential energy, which adds extra confirmation of the fundamental significance of Eq. (13). Equation (13) can be written in the form of macroscopic reduced units, $\tilde{u} = (\rho^4/T)\tilde{u}_r + (\rho^2/T)\tilde{u}_a$. Similarly, for the configurational part of the pressure, P_c, obtained from the virial expression, for the Lennard-Jones potential, $\tilde{P}_c = 4(\rho^4/T)\tilde{u}_r + 2(\rho^2/T)\tilde{u}_a$. However, these quantities do not display isomorphic collapse in the way the soft sphere fluid does, as the repulsive and attractive contributions are additive and depend differently on density as is obvious from Eq. (13). Nevertheless, quantities such as u, and P_c can be expressed as formulae of the form of Eq. (13), which implies that $\tilde{u}_r$ and $\tilde{u}_a$ should have a very weak density dependence (as may be shown for the present data).

Figure 14 presents the associated MD generated shear modulus, G_∞, bulk modulus, $K_\infty - K_0$, and thermal modulus, M_T associated with the shear and bulk viscosity and thermal conductivity Green-Kubo coefficients. The infinite frequency moduli for the LJ fluid is given by, [51, 58, 61, 69]

$$\begin{aligned} G_\infty &= \rho k_B T + \frac{\rho}{5}(36u_r + 6u_a) \\ K_\infty &= \frac{5}{3}\rho k_B T + \rho(20u_r + 6u_a) \end{aligned} \tag{15}$$

and hence

$$\tilde{G}_\infty = 1 + \frac{1}{5}(36\frac{\rho^4}{T}\tilde{u}_r + 6\frac{\rho^2}{T}\tilde{u}_a)$$

$$\tilde{K}_\infty = \frac{5}{3} + (20\frac{\rho^4}{T}\tilde{u}_r + 6\frac{\rho^2}{T}\tilde{u}_a) \quad (16)$$

These quantities follow u and P_c in being well represented by the function of the form $X = A\rho^4 - B\rho^2$. Least squares fits of the numerical data to this analytic form are shown as continuous curves on the figure. This result is because the infinite frequency elastic and thermal moduli can be expressed as the sum of two terms, one with a ρ^4 dependence (for the $n = 12$ part of the potential) and a ρ^2 term (for the $n = 6$ component), as for all similar mechanical and thermodynamic quantities.

The corresponding collective transport coefficients of shear and bulk viscosity, and thermal conductivity do *not* display MRU invariance with density as, although the relaxation times, τ, do exhibit good density invariance when expressed in this form (see Figs. 8-12), the moduli (as seen in Fig. 14) do not scale in this manner but according to the general expression given in Eq. (12). Nevertheless, the analytic form of the moduli along the isomorph can in principle be determined from two simulations using the analytic form of Eq. (12), which would make the transport coefficients along the fluid-solid boundary specified at each state point at coexistence. The self-diffusion coefficient is a special case as the equivalent of the modulus is then k_BT/m, so $D = k_BT\tau/m$. Figure 7 shows that there is an approximate invariance of $\tilde{D}$ at high density and temperature. Figure 15 shows that the MRU reduced infinite frequency shear modulus has a quite weak density dependence compared to the infinite frequency bulk modulus.

The **infinite frequency** elastic moduli are important in describing the propagation and absorption of sound, [50] in terms of the longitudinal modulus, $M_{\infty,L} = K_\infty + 4G_\infty/3$. For a liquid in which the atoms interact via a central or isotropic potential the Cauchy relationship,

$M_{\infty,L} = 3G_\infty$, is obeyed. Zwanzig and Mountain, [51, 64] derived a generalized Cauchy relationship for the Lennard-Jones fluid, using its analytic form introduced into the statistical mechanical definitions of the pressure, and shear and bulk moduli, which is,

$$M_{\infty,L} = 3G_\infty + 2P, \tag{17}$$

which was confirmed for the numerical data as it is exact for the LJ fluid. A more recent proposal for liquids close to the glass transition is the empirical formula, (see Refs. [64, 65] and references quoted therein)

$$M_{\infty,L} = a + bG_\infty. \tag{18}$$

which applies very well to the LJ fluid moduli along the fluid-solid coexistence line, as seen in Fig. 16. On the figure the abscissa are $M_{\infty,L} = K_\infty + 4G_\infty/3$ (open circles), and $M_{\infty,L} = 3G_\infty + 2P$ (crosses). The two should agree for the LJ potential, as they are seen to do within simmulation statistics. Typical values of b in the literature are close to 3, and the least squares fit to the present MD data gives a value of 3.8.

IV. CONCLUSIONS

Certain quantities when reduced according to so-called macroscopic-microscopic units (MRU) show the hallmarks of soft-sphere like isomorphism (*i.e.*, state point invariant) along the fluid-solid coexistence line. The radial distribution function exhibits very good MRU scaling which indicates that the coexisting fluid states along the Lennard-Jones fluid-solid coexistence line are essentially structurally isomorphic. The normalized time correlation functions scale very well also. These are properties which one might expect to be dominated by the repulsive part of the potential, and on the pair forces rather than the potential energy. The attractive part of the potential if approximated by a uniform background would not contribute to the force. The mean and root mean square force fall into this excellent MRU scaling category, as revealed in Fig. 6. Of all the density-temperature curves on the fluid part of the Lennard-Jones phase diagram that along fluid-solid coexistence is probably the most likely to exhibit structural isomorphism as this has the highest density at a given temperature, where one might expect the repulsive part of the potential to be most dominant. However, static quantities which are the sum of attractive and repulsive terms, such as the potential energy and pressure do not exhibit data collapse when expressed in terms of macroscopic reduced units as these two components have a different density dependence. Nevertheless, they can be expressed well as simple formulas such as the one in Eq. (13) for the potential energy per particle, u which follows *directly* from structural isomorphism to a good approximation. This suggests that $\tilde{u}_r$ and $\tilde{u}_a$, for example, are almost density independent, which is found to be the case.

The infinite frequency shear modulus is almost isomorphic in having a weak dependence on density when expressed in MRU, whereas the infinite frequency bulk modulus performs less well in this respect (see Fig. 14). As the infinite frequency elastic moduli can be written in

terms of integrals of the radial distribution function, [66, 67] and as these are to a very good approximation isomorphic states, one would expect these quantities to be expressible in the same generic form as the one in Eq. (13) for the potential energy per particle.

The assumption underlying perturbation theory,[68] is that the fluid structure is dominated by the repulsive or excluded volume part of the pair potential. **Because of the success of the general property formula of Eq. (12) for Lennard-Jones fluids, this might be construed that for the LJ fluid the r^{-12} part of the potential is the true reference state, which conflicts with the traditional assumption that the WCA potential is the most appropriate reference for the Lennard-Jones potential. In the WCA treatment the structure of the liquid is presumed to be determined essentially by an effective repulsive potential composed of a specific mixture of the r^{-12} and r^{-6} LJ terms. In Ref. [54] based on simulation results in that publication, the authors argue that what matters is the total force on the molecule which is determined by the local cage structure and therefore less obviously attributable to the details of a given pair potential. This issue is clearly one which would benefit from further investigation.** The isomorphic description provides **some useful additional** relationships (*e.g.*, see Eq. (12)) and extends our capability in specifying time dependent and hence linear (and possibly non-linear) rheological properties. The formalism of isomorphism provides new perspectives in our understanding and description of so-called van der Waals fluids (*i.e.*, not hydrogen bond dominated). There is 'hidden' scaling and simple relationships applicable to the Lennard-Jones fluid which have been established in some recent pioneering publications by other groups, and further explored for other properties, including elastic moduli, in this work. Isomorphism provides an explanation for a number of empirical trends of experimental data using MRU scaled variables noted over many decades. Of course,

the Lennard-Jones $\sim r^{-12}$ would be an approximation for the repulsive part of the potential for real molecular systems, in which case the more general relationship $\sim A\rho^{n/3} - B\rho^{m/3}$ for a given physical property could be fitted to experimental data, where n and m are treated as empirical constants. The $n : m$ potential form more immediately brings to light isomorphism characteristics, but this does not mean that extensions of this approach could not be extended to other repulsive potential forms, such as an exponential repulsion,[71] and the Morse potential.

The elastic moduli fall within the domain of structural isomorphism theory, as also found by others, [65]. Ultimately this way of analysing static and time-dependent physical properties may be useful in providing criteria which lead to, or at the very least compactly describe, auxetic behavior in small molecule liquid and solid systems.

In the field of tribology isomorphism has already been recognised as an important new development for high pressure or elastohydrodynamic lubrication (EHL) contacts, [72–74]. It is very difficult to carry out controlled experiments of the physical state of the lubricant in a working EHL contact zone. A small volume of lubricating oil may be in the contact zone for *ca.* 1 ms. There are large pressure gradients in the flow direction, and temperature gradients across the gap. Isomorphism theory could be used to provide a link between the high pressure states typical of EHL to low temperature ambient pressure states which are more readily probed by laboratory spectroscopic and viscometric equipment. Temperature then replaces pressure as the independent variable, which is less costly to vary than pressure (up to 2-3 GPa, typically) in a controlled manner.

References

[1] C.W. Smith and K.W. Wojciechowski, Phys. Stat. Solidi B 245, 486 (2008); K.L. Alderson, A. Alderson, J.N. Grima, K.W. Wojciechowski, Phys. Stat. Solidi B 251, 263 (2014); see also references therein.

[2] D.M. Heyes and A.C. Brańka, Soft Matter, **5**,2681, (2009).

[3] J.C. Maxwell, Phil. Trans. Roy. Soc. **157**, 49 (1867).

[4] C.M. Roland, S. Hensel-Bielowka, M. Paluch and R. Casalini, Rep. Progr. Phys. **68**, 1405 (2005).

[5] C.M. Roland, S. Bair and R. Casalini, J. Chem. Phys. **125**, 124508 (2006).

[6] D. Fragiadakis and C.M. Roland, J. Chem. Phys. **134**, 044504 (2011).

[7] D. Colsovich and C.M. Roland, J. Phys. Chem. B, **112**, 1329 (2008).

[8] C.M. Roland, R.B. Bogoslovov, R. Casalini, A.R. Ellis, S. Bair, S.J. Rzoska, K. Czuprynski and S. Urban, J. Chem. Phys. **128**, 224506 (2008).

[9] U.R. Pedersen, N.P. Bailey, T.B. Schrøder and J.C. Dyre, Phys. Rev. Lett. **100**, 015701 (2008).

[10] U.R. Pedersen, T.Christensen,T.B. Schrøder and J.C. Dyre, Phys. Rev. E. **77**, 011201 (2008).

[11] N.P. Bailey, U.R. Pedersen, N. Gnan, T.B. Schrøder, J.C. Dyre, J. Chem. Phys. **129**, 184507 (2008).

[12] N.P. Bailey, U.R. Pedersen, N. Gnan, T.B. Schrøder, J.C. Dyre, J. Chem. Phys. **129**, 184508 (2008).

[13] T.B. Schrøder, N.P. Bailey, U.R. Pedersen, N. Gnan, J.C. Dyre, J. Chem. Phys. **131**, 234503 (2009).

[14] N. Gnan, T.B. Schrøder, U.R. Pedersen, N.P. Bailey, J.C. Dyre, J. Chem. Phys. **131**, 234504 (2009).

[15] T.S. Ingebrigsten, T.B. Schrøder and J.C. Dyre, Phys. Rev. X **2**, 011011 (2012).

[16] L.A. Roed, D. Gundermann, J.C. Dyre and K. Niss, J. Chem. Phys. **139**, 101101 (2013).

[17] J.J. Potoff and A.Z. Panagiotopolous, J. Chem. Phys. **112**, 6411 (2000).

[18] J.Pérez-Pellitero, P. Ungerer, G. Orkoulas and A.D. Mackie, J. Chem. Phys. **125**, 054515 (2006).

[19] J. Mick, E. Hailat, V. Russo, K. Rushaidat, L. Schwiebert and J. Potoff, Comp. Phys. Comm. **184**, 2662 (2013).

[20] J. Kolafa and I, Nezbeda, Fluid Phase Eqilibria **100**, 1 (1994).

[21] M.A. Barroso and A.L. Ferreira J. Chem. Phys. **116**, 7145 (2002).

[22] S.A. Khrapak, M. Chaudhuri and G. E. Morfill, Phys. Rev. E **82**, 052101 (2010).

[23] S.A. Khrapak and G. E. Morfill, J. Chem. Phys. **134**, 094108 (2011).

[24] L. Separdar, N.P. Bailey, T.B. Schrøder, S. Davatolhagh and J. Dyre, J. Chem. Phys. **138**, 154505 (2013).

[25] L. Bøhling, T.S. Ingebrigsten, A. Grzybowski, P. Paluch, J.C. Dyre and T.B. Schrøder New J. Phys. **14**, 113035 (2012).

[26] R. Agrawal and D.A. Kofke, Phys. Rev. Lett. **74**, 122 (1995).

[27] R. Agrawal and D.A. Kofke, Mol. Phys. **85**, 43 (1995).

[28] E.A. Mastny and J.J. de Pablo, J. Chem. Phys. **127**, 104504 (2007).

[29] J.R. Morris and X. Song, J. Chem. Phys. **116**, 9352 (2002).

[30] M. A. van der Hoef, J. Chem. Phys. **117**, 5092 (2002).

[31] D.M. Heyes, S.M. Clarke and A.C. Brańka, J. Chem. Phys. **131**, 204506 (2009).

[32] M. Ross and B.J. Alder, Phys. Rev. Lett. **16**, 1077 (1966).

[33] A. Ahmed and R.J. Sadus, Phys. Rev. E **80**, 061101 (2009).

[34] V.G. Baidakov, S.P. Protsenko and Z.R. Kozlova, J. Chem. Phys. **137**, 164507 (2012).

[35] A. Lofti, J. Vrabec and J. Fischer, Mol. Phys. **76**, 1319 (1992).

[36] D.A. Kofke, J. Chem. Phys. **98**, 4149 (1993).

[37] G.C. McNeil-Watson and N.B. Wilding, J. Chem. Phys. **124**, 064504 (2006).

[38] A. Trokhymchuk, J. Chem. Phys. **111**, 4149 (1999).

[39] A. Ahmed and R.J. Sadus, J. Chem. Phys. **131**, 174504 (2009).

[40] Y. Rosenfeld, Phys Rev. A **15**, 2545 (1977).

[41] M.J. Assael, J.H. Dymond, M. Papadaki and P.M. Patterson, Int. J. Thermophys. **13**, 269 (1992).

[42] J.H. Dymond, Int. J. Thermophys. **18**, 303 (1997).

[43] N.H. March and J.A. Alonso, Phys. Rev. B **73**, 032201 (2006).

[44] J.J. van Loef, Physica B+C **124**, 305 (1984).

[45] D. Chandler, J.D. Weeks and H.C. Andersen, Science, **220**, 787 (1983).

[46] D. Coslovich and C.M. Roland, J. Phys. Chem. B Lett. **112**, 1329 (2008).

[47] S. Pieprzyk, D.M. Heyes and A.C. Brańka, Phys. Rev. E **90**, 012106 (2014).

[48] J.G. Powles and D.M. Heyes, Mol. Phys. **98**, 917 (2000).

[49] D.M. Heyes and P.J. Aston, J. Chem. Phys. **100**, 2149 (1994).

[50] W.M. Slie and W.M. Madigosky, J. Chem. Phys. **48**, 2810 (1968).

[51] R. Zwanzig and R.D. Mountain, J. Chem. Phys. **43**, 4464 (1965).

[52] D.M. Heyes: The liquid state - applications of molecular simulations (John Wiley & Sons, Chichester, 1998)

[53] H. Watanabe, N. Ito and C.-K. Hu, J. Chem. Phys. **136**, 204102 (2012).

[54] L. Bøhling, A.A. Veldhorst, T.S. Ingebrigtsen, N.P. Bailey, J.S. Hansen, S. Toxvaerd, T.B. Schrøder and J.C. Dyre, J. Phys. Cond. Matter, **25**, 032101 (2013).

[55] D. E. Albrechtsen, A. E. Olsen, U. R. Pedersen, T. B. Schrøder and J. C. Dyre, Phys. Rev. B **90**, 094106 (2014).

[56] U. Balucani and M. Zoppi, Dynamics of the liquid state, Clarendon Press, Oxford, 1994) p. 290.

[57] D.M. Heyes, J.G. Powles and G. Rickayzen, Mol. Phys., **100**, 595 (2002).

[58] D.M. Heyes, J. Chem. Soc. Faraday Trans. 2, **79**, 1741 (1983).

[59] Y. Rosenfeld, J. Chem. Phys. **63**, 2769 (1974).

[60] Y. Rosenfeld, J.E. Avron, S. Goshen and R. Thieberger, J. Chem. Phys. **66**, 2758 (1977).

[61] D.M. Heyes, J. Chem. Soc. Faraday Trans. 2, **80**, 1363 (1984).

[62] T.B. Schrøder, N. Ghan, U.R. Pedersen, N.P. Bailey, and J. C. Dyre, J. Chem. Phys. **134**, 164505 (2011).

[63] T.S. Ingebrigtsen, T.B. Schrøder and J. C. Dyre, J. Phys. Chem. B **116**, 1018 (2012).

[64] D. Fioretto, S. Corezzi, S. Caponi, F. Scarponi, G. Monacco, A. Fontana and L. Palmieri, J. Chem. Phys. **128**, 214502 (2008).

[65] C. Klieber, T. Hecksher, T. Pezeril, D.H. Torchinsky, J.C. Dyre and K.A. Nelson, J. Chem. Phys. **138**, 12A544 (2013).

[66] R.V. Gopala Rao and R. Venkatesh, Phys. Rev. A **39**, 9467 (1989).

[67] S. Hess, M. Kröger and W.G. Hoover, Physica A **239**, 449 (1997).

[68] S. P. Tan, H. Adidharma and M. Radosz, J. Phys. Chem. B **106**, 7878 (2002).

[69] R. Zwanzig, J. Chem. Phys. **43**, 714 (1965).

[70] S. Tøxvaerd and J.C. Dyre, J. Chem. Phys. **135**, 134501 (2011).

[71] A. K. Bacher, T. B. Schrøder and J. C. Dyre Nature Comm. **5**, 5424 (2014).

[72] S. Bair, C.M. Roland and R. Casalini, Proc. IMechE J. **221**, 801 (2007).

[73] S. Bair, Proc. IMechE J. **223**, 617 (2009).

[74] S. Bair, Proc. IMechE J. **224**, 2568 (2010).

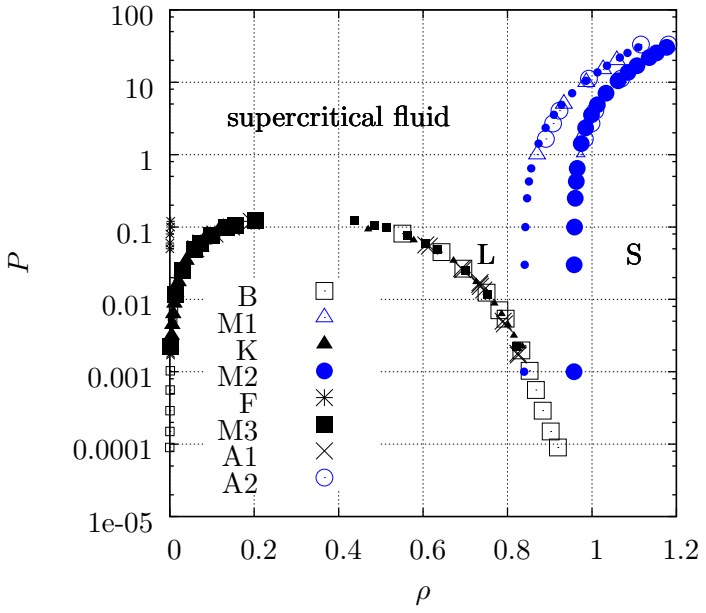

FIG. 1: Phase boundaries of the Lennard-Jones fluid system taken from a number of sources using Molecular Dynamics or Monte Carlo computer simulation. The figure shows pressure, P as a function of temperature, T. L denotes the solid region and L the liquid region. Note the lin-log scales. Key: References: [34] (B), [35] (F), [28] (M1) [36] (K), [37] (M2) [19] (M3), [17] (P), [38] (A1), and [39] (A2).

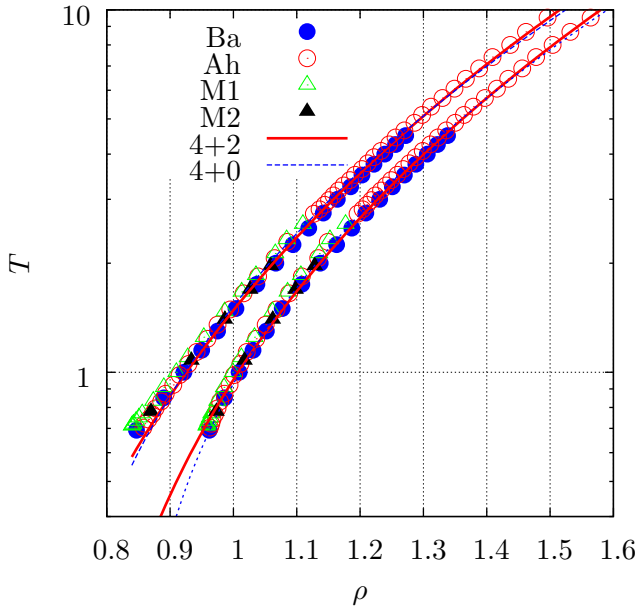

FIG. 2: The fluid and solid phase boundaries of the Lennard-Jones system using simulation data taken from various sources. The figure shows temperature, T, as a function of density, ρ. Key: References: [21] (Ba), [39] (Ah), [37] (M1), and [28] (M2). The constants in Eq. (1) for the $M42$ model are $A = 2.22(8)$ and $B = 0.74(12)$ for the liquid, and $A = 2.04(6)$ and $B = 1.09(10)$ for the solid. These best fit curves are indicated by '4+2' on the figure. Standard errors are reported here in brackets for the last digit(s) of the number. **This is the lower solid line for both liquid and solid data.** The constants in Eq. (3) for the $M40$ model are $C = -0.40(8)$ and $D = 1.92(4)$ for the fluid, and $C = -0.75(8)$ and $D = 1.68(3)$ for the solid. These best fit curves are indicated by '4+0' on the figure. **This is the upper solid line for both liquid and solid data.**

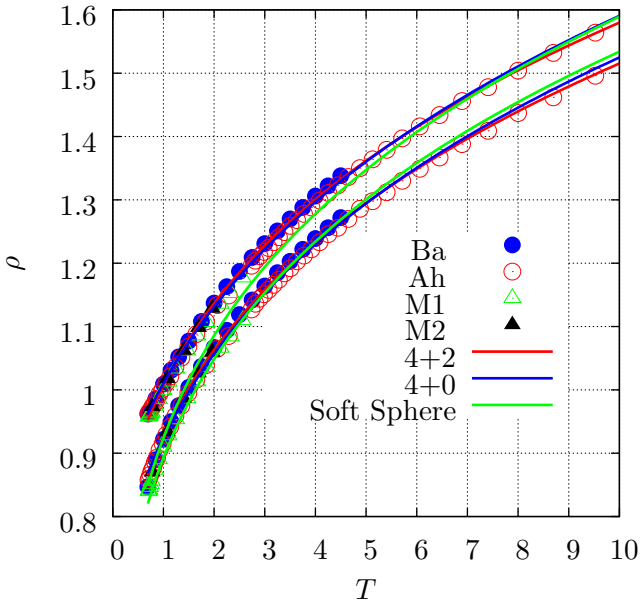

FIG. 3: As for Fig. 2 except that density, ρ, is plotted as a function of temperature, T. The $M42$ or '4+2' and $M40$ or '4+0 ' curves are the equations given in Eqs. (2) and (4), respectively. The two green lines ('Soft Sphere') are $0.8238T^{1/4} + 0.069$ and $0.8549T^{1/4} + 0.069$ (note the additional shift to the soft sphere formula) based on the soft sphere coexistence densities at $T = 1$ with data taken from Refs. [27, 31].

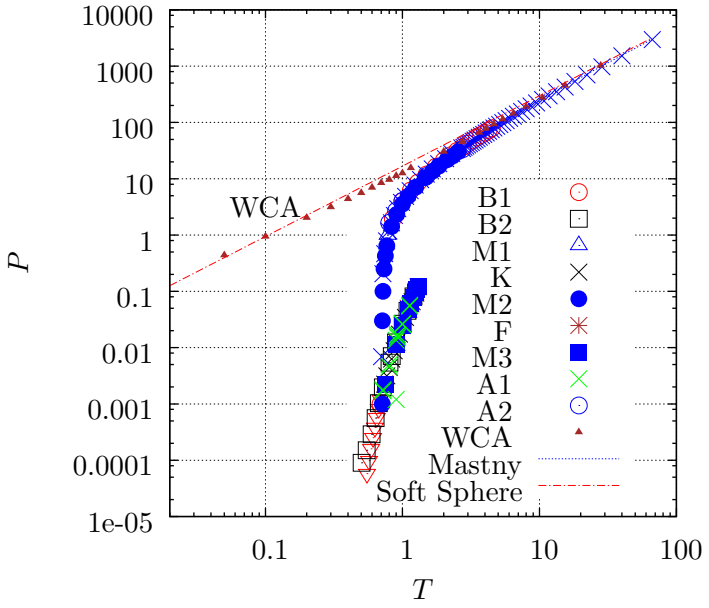

FIG. 4: The LJ pressure as function of temperature along the phase boundaries taken from various literature sources. The predominantly blue data point curve is for the fluid-solid coexistence, and the lower (green and red) points are for vapor-solid and vapor-liquid coexistence. Note the log-log plot. Key: References given on the figure: [34] (B), [35] (F), [28] (M1) [36] (K), [37] (M2) [19] (M3), [17] (P), [38] (A1), [21] (B2), and [33] (A2) for the WCA data points. 'Mastny' is taken from Ref. [28], and the solid red line labelled 'Soft Sphere is the $n = 12$ soft-sphere coexistence pressure, $P = 16.76\ T^{5/4}$ cast in LJ units and taken from Ref. [31].

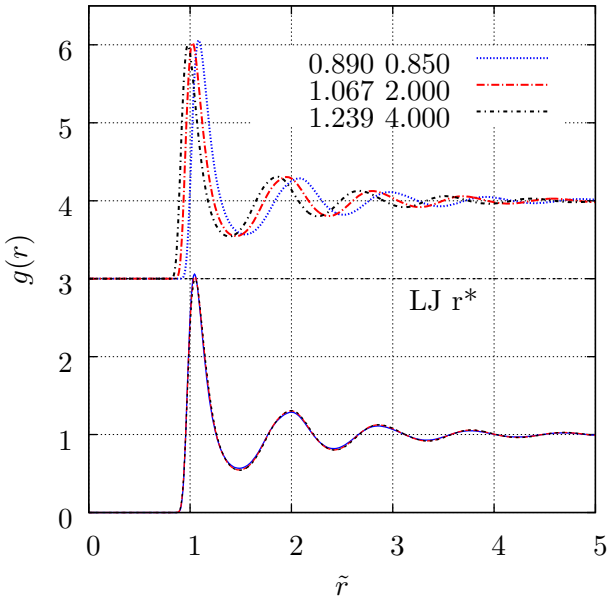

FIG. 5: Radial distribution function, $g(r)$ for three fluid states along fluid-solid coexistence. The numbers on the figure are ρ, T respectively in LJ time units. The top set of $g(r)$ are plotted with distance in LJ reduced units, and the bottom curves are the same data sets plotted using the macroscopically reduced distance, $\tilde{r}$.

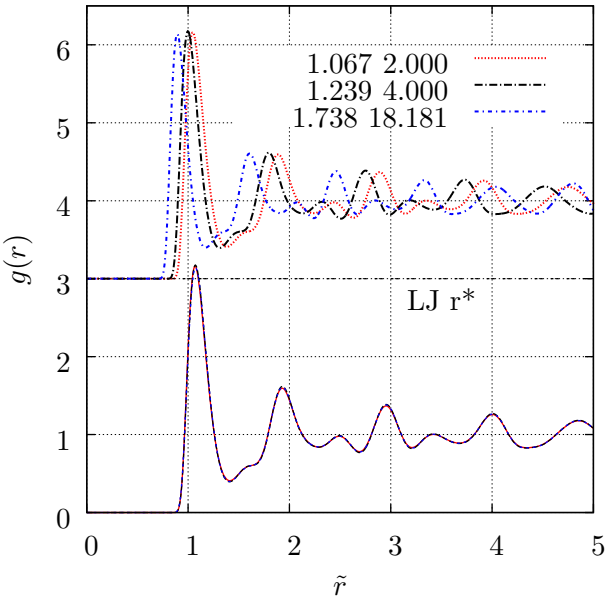

FIG. 6: As for Fig. 5 except that $g(r)$ for three solid states along fluid-solid coexistence are shown.

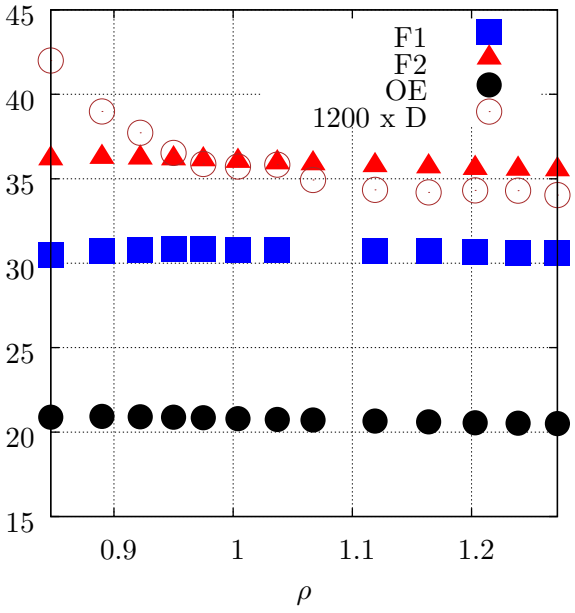

FIG. 7: Various macroscopically scaled properties plotted against ρ along the LJ fluid-solid phase boundary obtained by MD simulation. Key: mean force, $< \tilde{F} >$, (F1), root mean square force, $< \tilde{F}^2 >^{1/2}$, (F2), and Einstein frequency, $< \tilde{\omega}_E >$, (OE). The self-diffusion coefficient, $1200\times < \tilde{D} >$, (D), is also plotted. The letters in brackets are the annotation given on the figure.

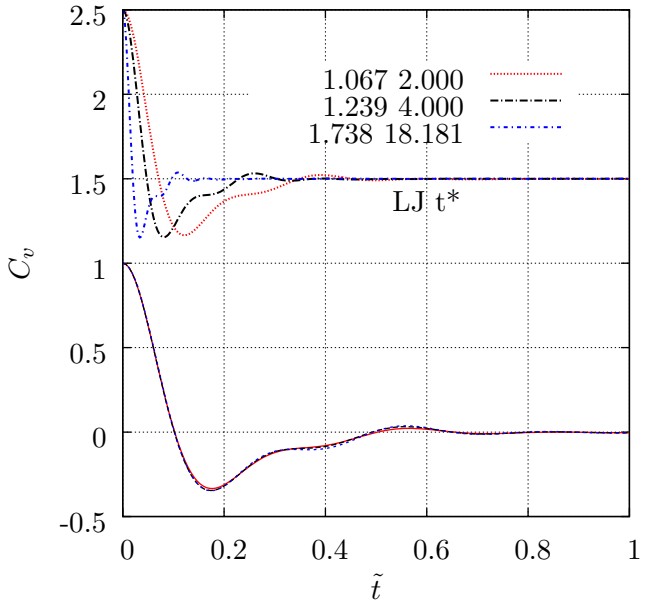

FIG. 8: Normalised velocity autocorrelation functions, $C_v(t)$ for three solid states along fluid-solid coexistence. The numbers on the figure are ρ, T in LJ time units. The top set of C_v are plotted with time in LJ reduced units, and the bottom curves are the same data sets plotted using the macroscopically reduced time, $\tilde{t}$.

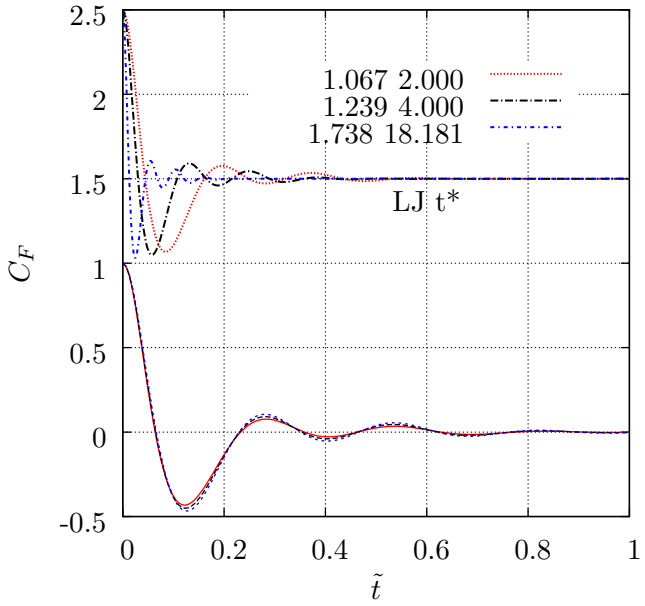

FIG. 9: As for Fig. 8 except the normalised force autocorrelation function, $C_F(t)$ is shown.

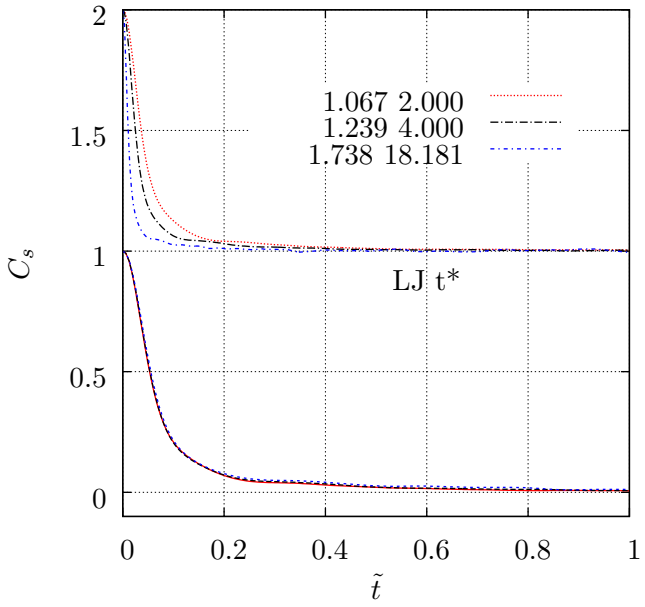

FIG. 10: As for Fig. 8 except the normalised shear stress autocorrelation function, $C_s(t)$ is shown.

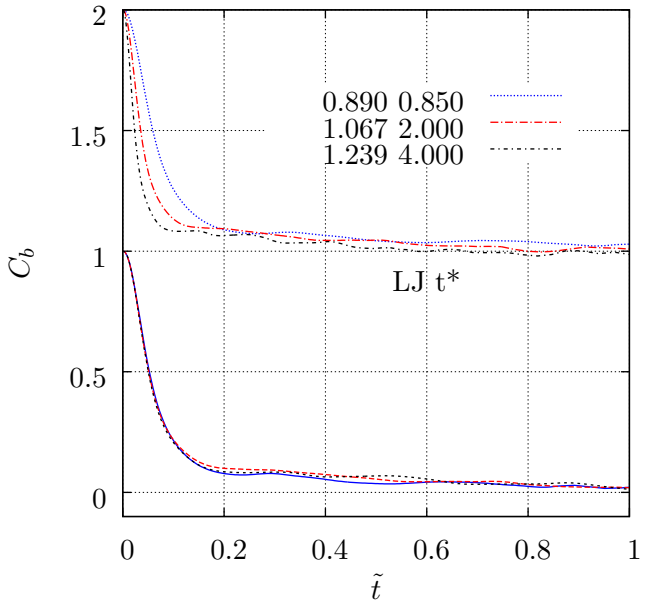

FIG. 11: The normalised deviatoric pressure autocorrelation function, $C_b(t)$ is shown for three fluid states.

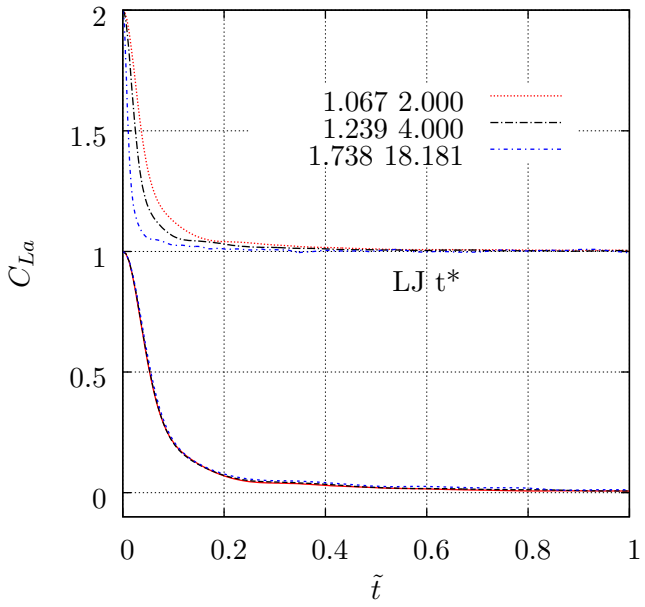

FIG. 12: As for Fig. 8 except the normalised heat flux autocorrelation function, $C_{La}(t)$ is shown.

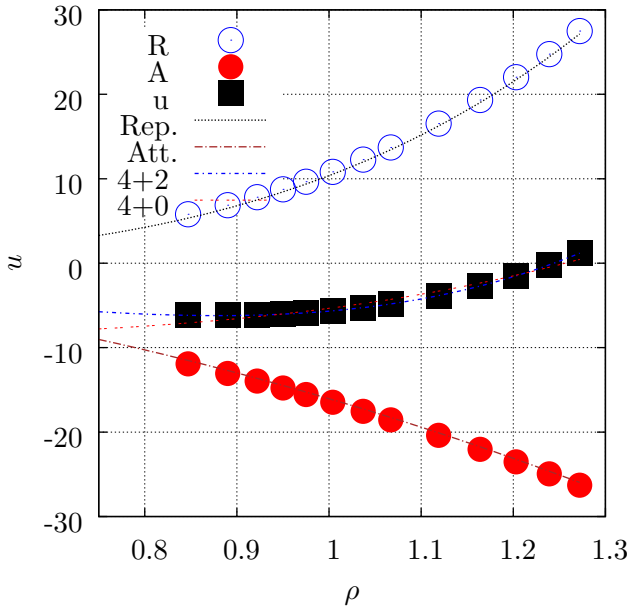

FIG. 13: The potential energy per particle, u, for the fluid LJ system along the fluid-solid phase boundary obtained by MD simulation. The contributions from the repulsive ('R') and attractive ('A') parts of the potential are given. Also the formula given in Eq. (13) fits the data very well. The black ($A_r\rho^4$) and brown ($B_a\rho^2$) lines are the components of this equation from the repulsive and attractive parts of the potential, respectively. The blue line is the formula in Eq. (13). A least squares fit gives $A_r = 10.37(1)$ and $B_a = 16.05(1)$ for Eq. (13), and $C_r = 3.6(2)$ and $D_a = 8.9(3)$ for Eq. (14).

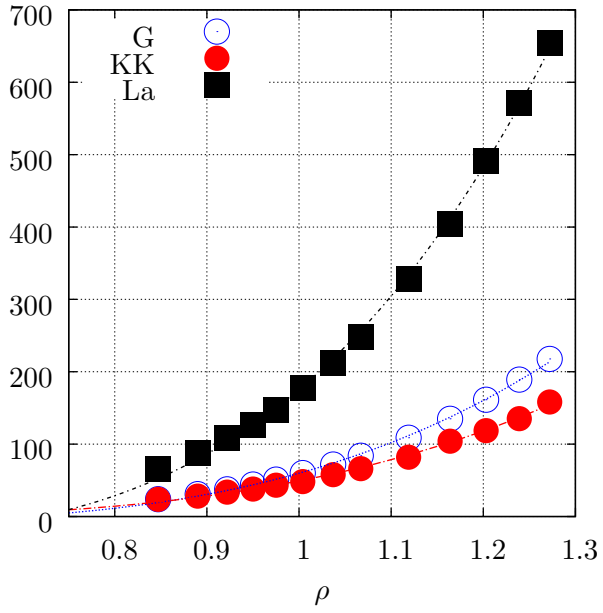

FIG. 14: The MD generated G_∞ (G), $K_\infty - K_0$ (KK) and M_T (La) as symbols for the coexisting fluid states, and their least square fit to functions of the form $X = A\rho^4 - B\rho^2$, which are continuous curves on the figure. For G: $A = 117(2),\ B = 57(3)$, for KK: $A = 75(2),\ B = -25(3)$, and for T: $A = 363(6),\ B = 187(8)$ (standard errors are in brackets).

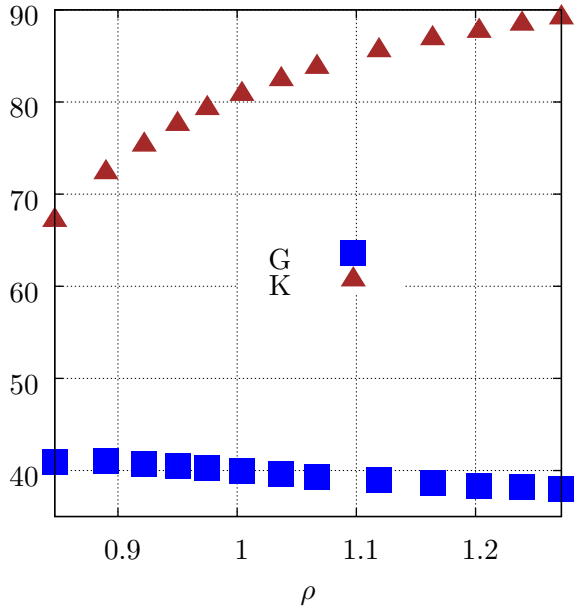

FIG. 15: The MD generated $\tilde{G}_\infty$ (G) and $\tilde{K}_\infty$ (K) as a function of number density for the LJ fluid states.

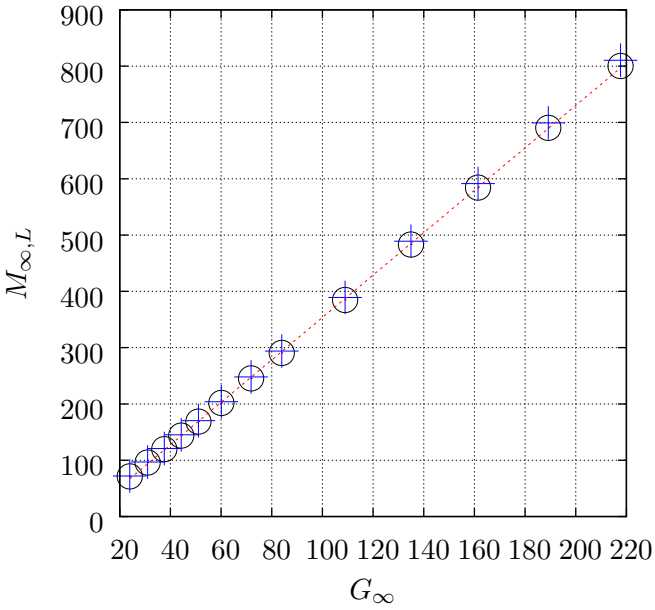

FIG. 16: Test of the formula given in Eq. (18) for the LJ MD data of the fluid along fluid-solid coexistence. Least square fit parameters are $a = -23(1)$ and $b = 3.77(1)$. The quantities are given in LJ reduced units. The open circles are $M_{\infty,L} = K_\infty + 4G_\infty/3$, and the crosses are $M_{\infty,L} = 3G_\infty + 2P$.

Acknowledgments

D.M.H. and D.D. acknowledge the support of the EPSRC Platform Grant EP/G026114/1.